JACS
JOURNAL OF THE AMERICAN CHEMICAL SOCIETY
pubs.acs.org/JACS
Article

Phase Control in the Synthesis of Iron Sulfides

Jeremy R. Bairan Espano and Janet E. Macdonald*

Cite This: J. Am. Chem. Soc. 2023, 145, 18948−18955
Read Online
ACCESS | Metrics & More | Article Recommendations | Supporting Information

ABSTRACT: The identity and repeating arrangement of atoms determine the properties of all solids. Even combinations of two atoms can have multiple crystal structures of varying stoichiometries and symmetries with vastly different electronic and chemical behaviors. The conditions of existing bottom-up routes for achieving one phase over another are serendipitous, and the links among precursor reactivity, decomposition mechanism, temperature, and time are elusive. Our studies take a systematic approach to understanding the role that the precursor kinetic decomposition has in the synthesis of iron sulfides, isolating it from other mechanistic factors. The data suggest that phase determination in binary solids can be logically predicted through the consideration of the anion stacking and thermodynamic relationships between phases. Mapping these relationships allows for the rational synthetic targeting of metastable crystalline phases.

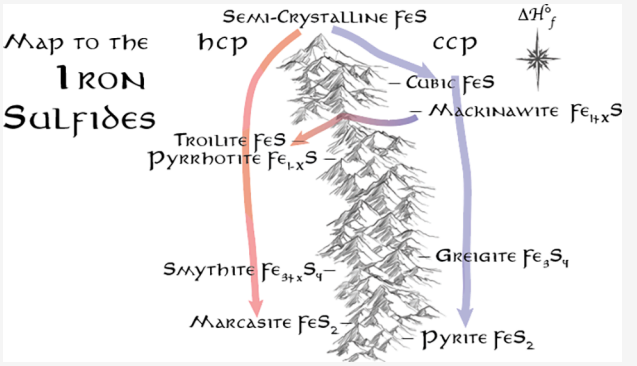

INTRODUCTION

The geological record demonstrates a diverse array of metal chalcogenides with varying compositions and crystal structures. For example, there are eight known geological iron sulfides (Table 1), four cobalt sulfides, seven nickel sulfides, and 10 copper sulfides. These compounds have myriad possibilities in technological applications because of their diverse electronic, optical, magnetic, chemical, and catalytic properties. However, these applications cannot be realized without reliable synthetic routes that can target each desired crystalline phase.

So far, there seems to be little progress on understanding how phases can be controlled in colloidal synthesis. While there are many one-off syntheses in the literature to individual metal sulfide phases, most are serendipitous without logical links between syntheses to other phases. When discussing synthetic routes, it is important to understand the intermediate phase "destinations" one can run into. There has been some progress; for example, Lennie et al.[2] mapped some of the pathways between iron sulfide phases in aqueous media, but the understanding is incomplete. In organic colloidal synthesis, even rudimentary synthetic maps of the phase space do not exist.

Rational phase control in bottom-up syntheses has not been completely understood, in part because the mechanisms of the molecular transformations that preclude crystal formation in solution have been mostly overlooked.[3−6] As well, systematic phase control studies that separated how fast from how a reaction occurs have not been performed. As an example, we studied the effect of organo-sulfur precursors on the phase of iron sulfide produced. Weaker S−C bond strength in the organo-sulfur reagents correlated with producing a phase with a higher sulfur content. However, a closer study of the reagent diallyldisulfide revealed that there was a decomposition mechanism different from that of the other reagents that uniquely facilitated pyrite formation.[7] Therefore, while there was a correlation between the availability of the S (through C−S bond strength) and the phase, the results were convoluted with how the particular reagents decomposed. What is needed is a series of reagents that decompose at varying rates without changing the decomposition mechanism.

Substituted thioureas are highly tunable in the rate at which they release sulfur. The number and identity of the substituents vary the rates of reactions in nanocrystal syntheses by several orders of magnitude.[3] Here, substituted thioureas in bottom-up syntheses are used as tunable sulfur reagents to study and isolate how reaction kinetics influence the phase of the resulting metal sulfides in bottom-up synthesis.

The iron sulfides are excellent target materials for a systematic study of phase control because the phase space is complex; there are known phases of several Fe/S stoichiometries of approximately 1:1, 3:4, and 1:2 with hexagonal and cubic polymorphs (Table 1). Many of the iron sulfides are of technological relevance in solar energy capture, magnetic storage, and biomedical applications.[8−10] While the iron sulfides have well-studied aqueous and geochemistry relevant

Received: June 5, 2023
Published: August 18, 2023

https://doi.org/10.1021/jacs.3c05653
J. Am. Chem. Soc. 2023, 145, 18948−18955

Table 1. Iron Sulfides

phase	chemical formula	space group	approximate sulfur packing	cation hole filling	ΔS_f (J/mol K)	ΔH_f (kJ/mol)	reference author
pyrite	FeS_2	*Pa*3	S_2^{2-} in ccp	all Oh	52.9	−171.5, −171.1, −173.6.	Waldner,[12] Grønvold,[13] Anderko,[14] Chase[15]
marcasite	FeS_2	*Pnnm*	S_2^{2-} in hcp	all Oh	62.4	−169.5	Grønvold,[13] Anderko[14]
troilite	FeS	*P*62*c*	S^{2-} in hcp	all Oh	50.5, 60.3	−101.4, −100.1	Waldner,[12] Anderko,[14] Chase,[15] Vaughan[16]
mackinawite	$Fe_{1+x}S$	*P*4/*nmm*	S^{2-} in ccp	Td (in layers)	64.4	−91.6	Berner,[17] Anderko,[14] Chase[15]
cubic iron sulfide	FeS	$F\bar{4}3m$	S^{2-} in ccp	1/2 Td (zinc blende-like)		>−91.6[a]	de Médicis[18]
greigite	Fe_3S_4	*Fd*3*m*	S^{2-} in ccp	all Oh, 1/2 Td (spinel)	63.4	−144.1, −141.2	Subramani,[19] Hoffmann[20]
smythite	$Fe_{3+x}S_4$	*R*3*m*	S^{2-} in hcp	All Oh, 1/2 Td		∼−150%	Erd[21]
pyrrhotite	$Fe_{1-x}S$	$P12_1/c$	S^{2-} in hcp	Oh (with vacancies)	60.3	−106.2	Anderko,[14] Chase[15]

[a]Based on the observation that cubic iron sulfide decomposes to mackinawite. Materials project database has calculated that the enthalpy of formation for smythite is slightly more negative than that of greigite.[1]

to minerology and the study of the origins of life, the overarching themes to phase trends are elusive.[11]

Here, we employ the use of tunable thioureas in a bottom-up synthesis. By doing so, we identified all eight of the known geological iron sulfides [pyrite (FeS_2), marcasite (orthorhombic, *o*-FeS_2), greigite (Fe_3S_4), smythite ($Fe_{3+x}S_4$), mackinawite ($Fe_{1+x}S$), pyrrhotite ($Fe_{1-x}S$), troilite (FeS), and cubic iron sulfide (FeS)]. These experiments allowed for the mapping of the kinetic, thermodynamic, and crystalline relationships between the phases, adding a layer of understanding to the existing literature preparations of these phases. Analyzing these results shows that anion stacking structure plays a determining role in nanocrystalline growth and phase transformations. Here, we show that the identified relationships can be used to make hypothesis-driven changes to the synthetic conditions to target specific phases. The way we rationalize and strategize synthetic pathways in bottom-up synthesis is a new approach and way of thinking about nanocrystalline synthesis.

RESULTS AND DISCUSSION

Iron sulfides were synthesized by heating a solution of iron(III) stearate ($Fe(C_{18}H_{37}CO_2)_3$, 0.5 mmol) in octadecene (ODE) to the desired reaction temperature (170−245 °C). A solution of substituted thiourea (3 mmol) in ODE (either at a Fe/S molar ratio of 1:3 or 1:6) was heated to a matching temperature before being added swiftly to the reaction flask (Figure 1a). Throughout the different iron sulfide syntheses, a stoichiometric excess of thiourea is employed. This allows the thiourea to release sulfur as a monomer for nanocrystal formation and also as a redox flexible species, as both the iron ($Fe^{3+/2+}$) and sulfur (S_2^{2-}/S^{2-}) oxidation states vary in the known iron sulfides.

To determine the extent to which kinetics plays a role in a phase control phenomenon, a library of thioureas were employed with differing conversion rates. The Owen group used slow reaction kinetics (over minutes) and in situ UV−vis to follow the synthesis of PbS nanocrystals.[3] We use two of the same thioureas as the Owen group but add on some more reactive species as well. A direct application of their approach to follow the reactions is not possible for the iron sulfides since there are multiple possible nucleating phases, each with their own absorption profiles. Instead, we use the ^{13}C NMR chemical shift of the C═S as a measure of the electron density on the carbon and adjoining sulfur. From the ^{13}C NMR, we infer the reactivity order to follow: thiourea (**1**) > methylthiourea (**2**) > acetylthiourea (**3**) > phenylthiourea (**4**) > 1-3,5-bis(trifluoromethyl)phenyl-3-phenyl-2-thiourea (**5**) > diphenylthiourea (**6**) (Figure 1a). Extrapolating from the Owen work, we approximate this library covering several orders of magnitude of conversion rate.

After isolation through successive precipitation and dispersion with ethanol and chloroform, all solid products were analyzed by powder X-ray diffraction with Rietveld refinements of the pattern (Supporting Information Table S1). Powder XRD has a limit of detection of about 1−2% composition by volume. Many of the products in these experiments were nanocrystalline with broad peaks, further increasing the limit. In some reactions, the products were phase pure within the limits of powder XRD experiments, while in others, a complex mixture of phases resulted. Marcasite (*o*-FeS_2), pyrite (FeS_2), mackinawite ($Fe_{1+x}S$), smythite ($Fe_{3+x}S_4$), cubic iron sulfide, greigite (Fe_3S_4), pyrrhotite ($Fe_{1-x}S$), and semicrystalline FeS were all identified as products (Figure 1c: 170 °C, d: 195 °C, e: 220 °C, f: 245 °C; the explicit percentages are included in the Supporting Information). Refinements were performed using Rigaku PDXL2 software, and the PDF files are noted in Figure 1. Quantification of semicrystalline FeS was obtained by assuming that the (001) of macknawite (17.61°) has a similar reflection of semicrystalline FeS (16.68°).

To the best of our knowledge, this is the first time all of the known geological iron sulfides have been synthesized in a single set of systematically varied experimental conditions. A synthetic phase diagram was created to illuminate the intersectionality of reaction conditions and phases (Figure 1f). At the lower synthetic temperatures < 200 °C, mixtures of smythite ($Fe_{3+x}S_4$), cubic iron sulfide (FeS), troilite (FeS), mackinawite ($Fe_{1+x}S$), and greigite (Fe_3S_4) were synthesized with the fastest-reacting thioureas. The low temperatures and fast-reacting thioureas work in concert to kinetically trap these phases with small $\Delta H°_f$ (Table 1) (we ignore the influence of ΔS_f since the standard enthalpies of formation ΔS_f are similar throughout the family of iron sulfides (50−64 J/mol K). The difference in the value of the ΔS contribution to ΔG is at most 7 kJ/mol (between mackinawite and troilite) at the highest synthetic temperature of 245 °C, which is smaller than the ΔH contribution.) When using slower-reacting thioureas at the low temperatures, greigite (Fe_3S_4) was the dominant product, which has the next largest negative $\Delta H°_f$—with some remaining mackinawite ($Fe_{1+x}S$) for the very slowest-reacting thioureas.

https://doi.org/10.1021/jacs.3c05653
J. Am. Chem. Soc. 2023, 145, 18948−18955

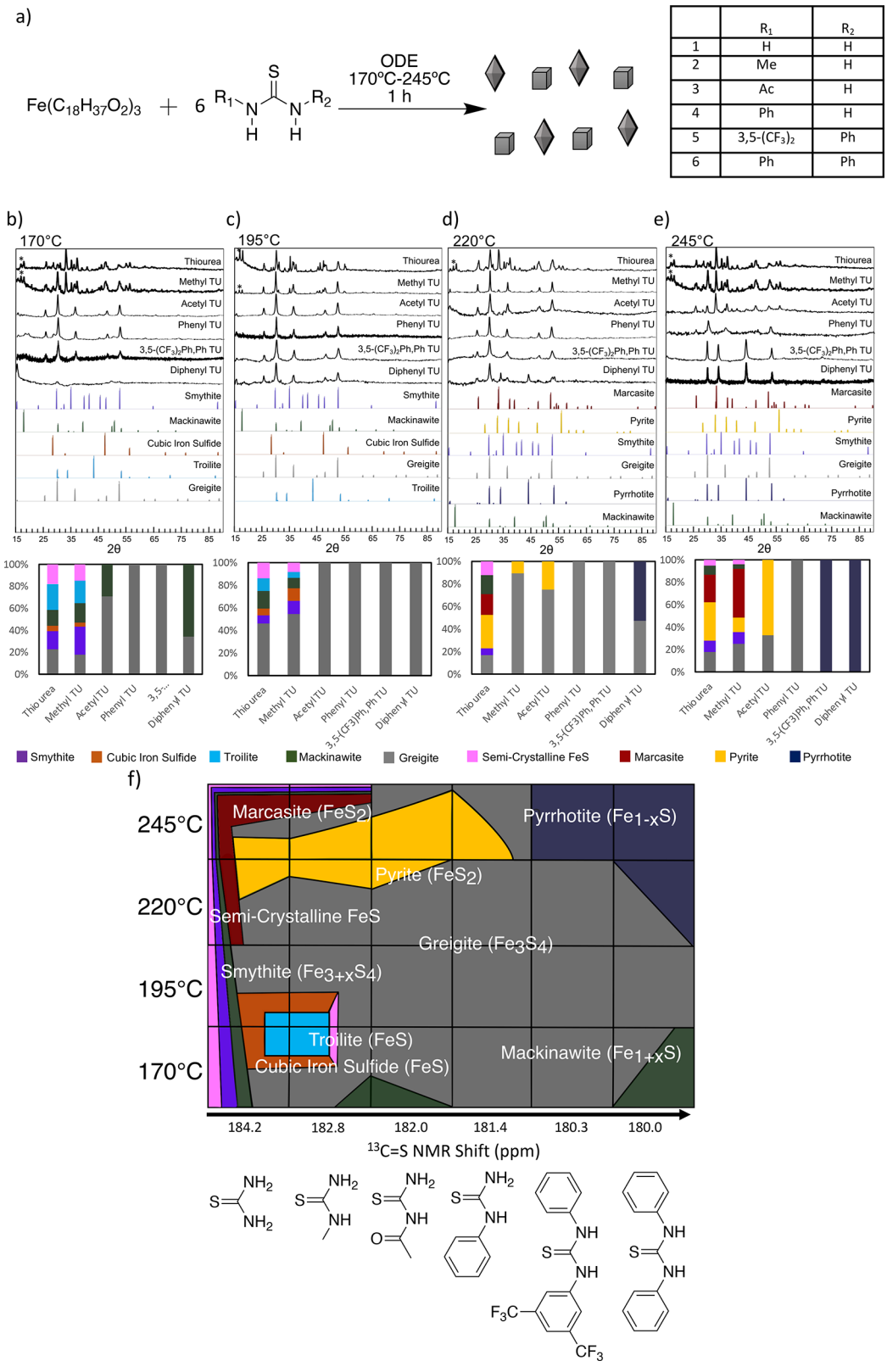

	R_1	R_2
1	H	H
2	Me	H
3	Ac	H
4	Ph	H
5	3,5-$(CF_3)_2$	Ph
6	Ph	Ph

Figure 1. (a) Schematic of the solution phase synthesis of various crystalline phases of iron sulfides using substituted thioureas (TU) as sulfur reagents. Powder X-ray diffraction (XRD) of the products and percent compositions at synthetic temperatures of (b) 170 °C, (c) 195 °C, (d) 220 °C, and (e) 245 °C. (ICSD smythite: 900077, troilite: 68852, mackinawite: 182250, greigite: 160713, marcasite: 9013067, pyrite: 10422, pyrrhotite: 240220, cubic iron sulfide reference powder obtained from Médicis et al., semicrystalline FeS reference powder obtained from Pósfai et al. and Benning et al. denoted *, Supporting Information Table S1). (F) Bottom-up, synthetic phase diagram representing the approximate compositions of the generated phases gathered from the XRD patterns above. The *X*-axis represents the substituted thioureas used in the iron sulfide synthesis, ranging from most reactive thiourea on the left to least reactive thiourea on the right as judged by the $^{13}C{=}S$ chemical shift.

https://doi.org/10.1021/jacs.3c05653
J. Am. Chem. Soc. 2023, 145, 18948−18955

Increasing the reaction temperatures to >200 °C afforded different phase mixtures but with generally more negative ΔH°_{f} and higher sulfur content than at the lower temperatures. Fast-reacting thioureas (thiourea and methylthiourea) yielded a mixture of smythite ($Fe_{3+x}S_4$), pyrite (FeS_2), marcasite (*o*-FeS_2), and greigite (Fe_3S_4). Medium-reacting thioureas (acetylthiourea and phenylthiourea) yielded a mixture of pyrite (FeS_2) and greigite (Fe_3S_4). Slow-reacting thioureas (1-3,5-bis(trifluoromethyl)phenyl-3-phenyl-2-thiourea and diphenylthiourea) yielded a mixture of greigite (Fe_3S_4) and pyrrhotite ($Fe_{1-x}S$). As the reaction temperature was further increased to 245 °C, pyrite (FeS_2), marcasite (*o*-FeS_2), and pyrrhotite ($Fe_{1-x}S$) became more dominant.

The synthetic phase diagram was prepared to aid in visualization of results (Figure 1f) where each box is colored to represent the approximate ratios of phases observed. The diagram highlights both intuitive and unexpected relationships. It is not surprising that to achieve the most sulfur-rich phases, FeS_2 pyrite (FeS_2) and marcasite (*o*-FeS_2), a temperature greater than 200 °C and fast-reacting thioureas are needed.[22] But curious anomalies also become apparent. For example, with slow-reacting thioureas, low temperatures give greigite (Fe_3S_4), but increasing the temperature causes the exclusive formation of a more sulfur-poor phase, pyrrhotite ($Fe_{1-x}S$).

The results are highly complex at first glance. Upon considering the thermodynamic stability of the phases, and splitting them into two categories—those based on approximate ccp and hcp stacking of the anions—explanations for the results clarify and are consistent with many of the observations of phase transformations made by the mineralogical and solid-state communities.[2,23−28]

We build from Ostwald's 1897 "Rule of Stages" observation that when multiple polytypes are possible (phases of the same stoichiometry but different arrangements of atoms), metastable phases form first and then transform into more thermodynamically stable phases.[29] More recently, it has been postulated that the metastable phases are actually the thermodynamically more stable phase at small nuclei sizes where surface energy dominates the thermodynamics.[29,30] In the iron sulfur family, there are several hexagonal/cubic polymorphic pairs of similar composition [troilite (FeS)/mackinawite ($Fe_{1+x}S$), smythite ($Fe_{3+x}S_4$)/greigite (Fe_3S_4), and FeS_2 marcasite (*o*-FeS_2)/pyrite (FeS_2)], but transformation between polytypes is usually not observed. Instead, under forcing conditions such as elevated temperatures and additional sulfur content, phases are transformed to one of a differing stoichiometry rather than one with a different polytype.[2,23−28]

Here, we build from Ostwald's postulate and add that the ccp or hcp stacking of the anions in the nucleated phase is a key determinant in the subsequent phase transformations to phases of differing stoichiometry. The iron sulfides can be imagined as two enthalpic "valley paths", dictated by their anion packing in the thermodynamic landscape separated by a high-activation-energy "mountain range." Troilite (FeS), pyrrhotite ($Fe_{1-x}S$), smythite ($Fe_{3+x}S_4$), and marcasite (*o*-FeS_2) all have approximate hcp stacking of the anions, either as S^{2-} or S_2^{2-} in the case of marcasite (*o*-FeS_2). In contrast, cubic iron sulfide (FeS), mackinawite ($Fe_{1-x}S$), greigite (Fe_3S_4), and pyrite (FeS_2) all have approximate ccp stacking (with pyrite having S_2^{-2} units) (Figure 2).

Of all of the phases, cubic FeS is the highest energy, and Ostwald's rule of stages suggests that this local minimum will be found first.[29] Under conditions where excess sulfur can be

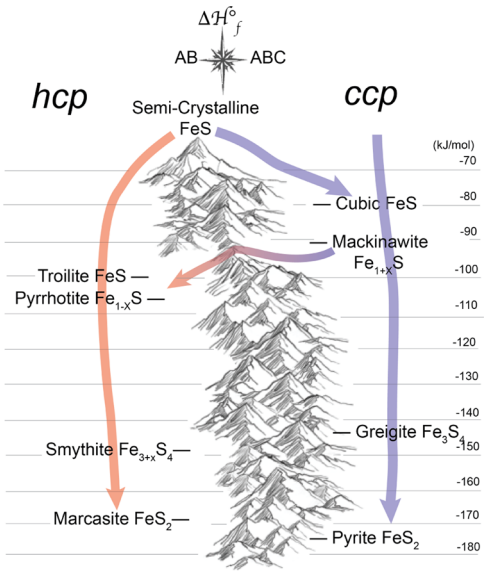

Figure 2. Map that describes the synthetic transformations in colloidal synthesis.

incorporated, the nucleation of the ccp cubic FeS leads down the ccp path to mackinawite ($Fe_{1+x}S$), greigite (Fe_3S_4), and then pyrite (FeS_2). Transformation of the ccp lattice to hcp is kinetically hindered,[31] even though there are hcp phases of intermediate enthalpy. The reactivity of the medium-reacting thioureas (acetylthiourea and phenylthiourea) provides an example of how nucleation in the ccp stacking forces a specific path of phase transformations. At low temperatures, the metastable ccp structure mackinawite ($Fe_{1-x}S$) resulted. With elevated reaction temperature and excess thiourea reagents, only greigite (Fe_3S_4) resulted, suggesting that any nucleated ccp mackinawite ($Fe_{1+x}S$) was transformed to ccp greigite (Fe_3S_4), skipping hcp troilite (FeS), or pyrrhotite ($Fe_{1-x}S$), even though they are of intermediate thermodynamic stability. Only at the highest temperatures was additional sulfur incorporated to cause ccp pyrite (FeS_2) to form, and again, there was no evidence that the next thermodynamic steps of hcp smythite ($Fe_{3+x}S_4$) or hcp marcasite (*o*-FeS_2) formed as intermediates.

The concentrations of each of the thioureas were halved for a series of reactions at 220 °C (Supporting Information). In comparison to the full 6:1 ratio (Figure 1d), unsurprisingly, the sulfur-rich phases of pyrite and marcasite (FeS_2) were absent from the products. However, like the reactions with high concentrations, at low concentrations, the fastest thiourea still gave a mixture of hcp and ccp products (troilite FeS and greigite Fe_3S_4, respectively), and the intermediate reacting thioureas all gave only ccp products (greigite Fe_3S_4). With the slowest-reacting thioureas, only pyrrhotite (hcp, $Fe_{1-x}S$) was obtained, instead of a mixture with greigite (Fe_3S_4), further indicating that sulfur incorporation into sulfur-rich phases is hindered.

The paths of the ccp phases have been studied previously under aqueous conditions showing interconversion, avoiding the hcp phases.[2,23−28] Hunger et al. reported that under sulfur-limited conditions, a mixture of mackinawite ($Fe_{1+x}S$), greigite (Fe_3S_4), and pyrite (FeS_2) can be observed and not the hcp phases.[25] With sulfur as an oxidant, mackinawite ($Fe_{1+x}S$) can transform to pyrite (FeS_2), with greigite (Fe_3S_4) hypothesized as an intermediate.[25] Greigite ($Fe^{2+}Fe_2^{3+}S_4$) can transform to

https://doi.org/10.1021/jacs.3c05653
J. Am. Chem. Soc. 2023, 145, 18948−18955

pyrite ($Fe^{2+}S_2^{2-}$), with the formation of persulfide resulting from a coupled reduction of ferric irons and the oxidation of sulfide ions.[32] In general, the ccp phases, pyrite (FeS_2) and greigite (Fe_3S_4), dominate the synthetic literature (with the exception of pyrrhotite ($Fe_{1-x}S$), vide infra) and are readily synthesized. It can be hypothesized then that the high-energy local minima of cubic FeS and mackinawite ($Fe_{1+x}S$) make the ccp valley the "path most traveled".

In nature and in synthetic studies, the hcp family of iron sulfide phases is much more difficult to achieve. The exception is pyrrhotite ($Fe_{1-x}S$), which forms under conditions with high temperatures and a low sulfur content.[31] The more sulfur-rich hcp smythite ($Fe_{3+x}S_4$) and marcasite (o-FeS_2) are very rare in nature, forming most often when templated onto other hcp minerals such as siderite ($FeCO_3$) or nickel sulfide, which lowers their surface energy.[27] Some recent theoretical calculations have hinted that at low pH and small size, marcasite (o-FeS_2) is actually more stable than pyrite (FeS_2) because it has a lower surface energy.[33]

In this study, the hcp family of phases were conucleated with the ccp family of phases under highly reactive conditions with the fastest-reacting thioureas (Figure 3). Even at 170 °C, where conversion from mackinawite to pyrrhotite is kinetically hindered,[31] hcp phases were observed. Several groups have recognized that fast aqueous precipitations to iron sulfides can lead to an intermediate semicrystalline FeS phase[34−36] which can anneal into both ccp mackinawite or hcp pyrrhotite < 150 °C. This is similar to a semiamorphous phase of Ni_2P which forms before crystallization of hexagonal Ni_2P in colloidal synthesis.[37] Here, the fast-reacting thioureas also caused the formation of the semicrystalline phase, which was identified by XRD (Figure 1*) but was not observed with the slower-reacting thioureas.

In these experiments, the semicrystalline FeS intermediate caused indiscriminate nucleation into both the ccp path [cubic FeS to mackinawite ($Fe_{1+x}S$), greigite (Fe_3S_4), and pyrite (FeS_2)] and the hcp path [troilite (FeS) to pyrrhotite ($Fe_{1-x}S$), smythite ($Fe_{3+x}S_4$), and marcasite (o-FeS_2)]. Extending the reaction time fully transforms the mixture into marcasite (o-FeS_2) and pyrite (Figure 3). The indiscriminate nucleation into the amorphous intermediate with highly reactive sulfur precursors will, therefore, create a mixture of hcp and ccp phases.

The hcp family was also approached through a second route, which led to increased phase purity and revealed a high temperature route between the ccp and hcp paths. Reactions with slow-reacting thioureas ensured the formation of ccp nuclei, initiating the cubic path through mackinawite ($Fe_{1-x}S$) to greigite (Fe_3S_4). Increasing the temperature should increase the reactivity of the thiourea to encourage pyrite (FeS_2) formation. However, at 245 °C, pyrrhotite ($Fe_{1-x}S$) instead formed. An energetic barrier from ccp mackinawite ($Fe_{1+x}S$) to hcp pyrrhotite ($Fe_{1-x}S$) can be considered a "low mountain pass" between the ccp and hcp valleys. 245 °C provides enough thermal energy for ccp mackinawite ($Fe_{1+x}S$) nuclei to transform to the more thermodynamically stable polytype hcp pyrrhotite ($Fe_{1-x}S$).[31]

At 245 °C, after crossing the mountain pass, the hcp pyrrhotite ($Fe_{1-x}S$) was kinetically trapped; hcp smythite ($Fe_{3+x}S_4$) did not form, even though its ccp cousin greigite (Fe_3S_4) can form under milder conditions on the ccp path. The lowered starting enthalpy of pyrrhotite ($Fe_{1-x}S$) compared with that of mackinawite ($Fe_{1+x}S$) creates a larger and

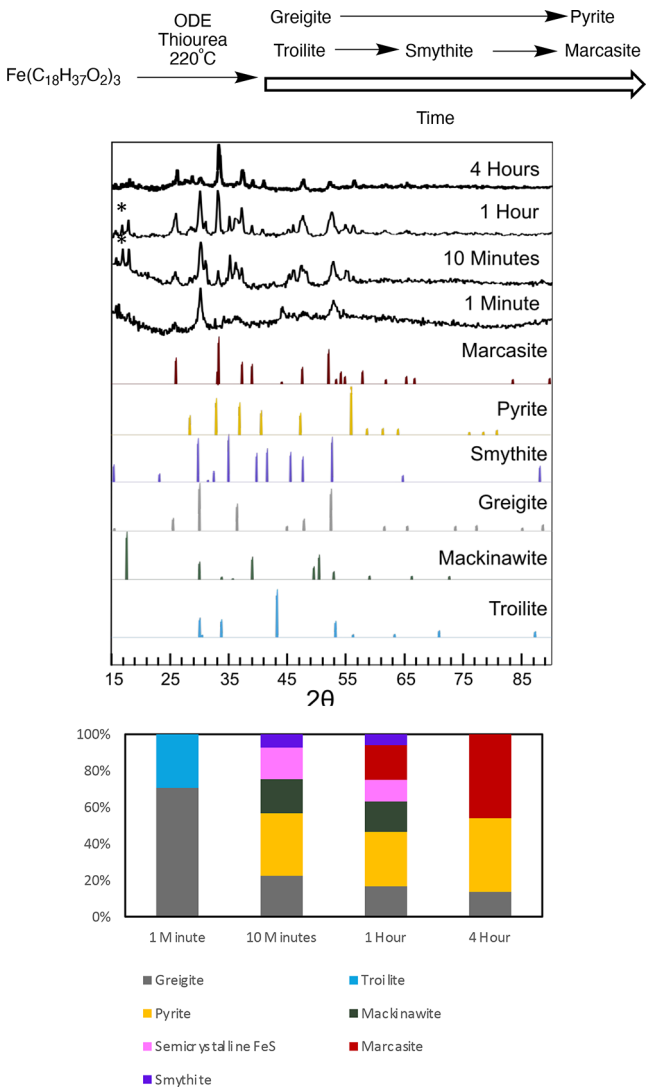

Figure 3. Progression of the iron sulfide phase with time. XRD of the products and standard patterns (ICSD marcasite: 9013067, pyrite: 10422, smythite: 900077, greigite 160713, troilite 68852) * denotes a semicrystaline FeS phase[34]

hindering activation energy to continue adding sulfur on the hcp path to smythite ($Fe_{3+x}S_4$) and marcasite (o-FeS_2).

With the developed phase map in hand, it is possible to target phases that are elusive due to either their metastability or their sulfur anion packing. By taking into account both chemical toolkits as well as crystalline pathways, we can strategize how to navigate between the iron sulfide phases. Below are pioneering cases where instead of serendipitous, rational phase control can be achieved (Figure 4).

Conditions to Mackinawite. Mackinawite ($Fe_{1-x}S$) is a highly metastable phase that is typically prepared from aqueous precipitations. At temperatures below 100 °C, it can be sulfurized to give the ccp phases greigite (Fe_3S_4) or pyrite (FeS_2).[11] A preparation of pure mackinawite ($Fe_{1+x}S$) in organic media is not known but now can be targeted using information from the developed phase diagram. The synthetic phase diagram indicates that greigite (Fe_3S_4) is grown by using slow-reacting thioureas at temperatures below 200 °C, and it can be hypothesized that further slowing the reactivity of the thiourea will lead to isolation of mackinawite ($Fe_{1+x}S$). Therefore, very unreactive 1-hexyl-3-phenyl-2-thiourea was

https://doi.org/10.1021/jacs.3c05653
J. Am. Chem. Soc. 2023, 145, 18948−18955

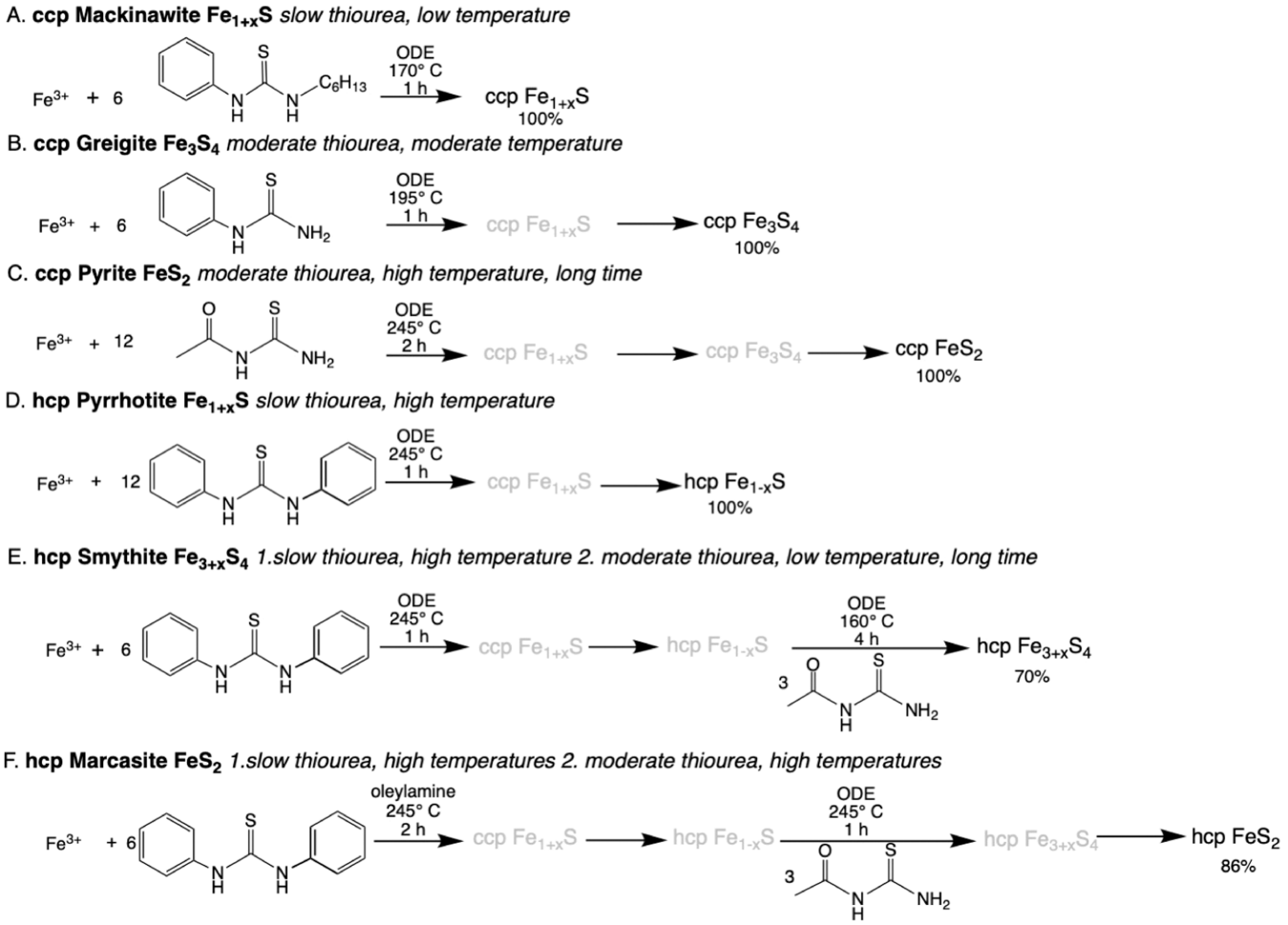

Figure 4. Rational syntheses of six iron sulfides. Gray compounds are presumed and nonisolated intermediates.

synthesized and used for nanocrystal synthesis at 170 °C, which yielded pure mackinawite ($Fe_{1+x}S$) within the limitations of quantification by pXRD. Similarly, slow reactions and the trapping of mackinawite ($Fe_{1+x}S$) can be facilitated by employing a coordinating solvent to lower surface energy, while slower thioureas at 170 °C predominately yielded a mixture of greigite (Fe_3S_4) and mackinawite ($Fe_{1+x}S$) in ODE (Supporting Information).

Conditions to Synthesize Greigite and Pyrite. Pyrite (FeS_2) is the most thermodynamically stable phase in the iron sulfide library but is often synthesized with impurities of its hexagonal counterpart marcasite (o-FeS_2). We can hypothesize that this can be prevented by keeping temperatures below the pass between ccp and hcp valleys and using slow thioureas to favor nucleation into the ccp path. The initial study showed that ccp greigite (Fe_3S_4) can be achieved by using a medium-reacting thiourea, such as acetylthiourea or phenylthiourea, at 195 °C. Under these conditions, more sulfur needs to be included to follow the ccp valley to pyrite. Raising the temperature to 245 °C, doubling the molar ratio of acetylthiourea/Fe to 12:1, and doubling the reaction time to 2 h, gave pyrite (FeS_2) as the only identified iron sulfide by XRD.

Accessing the HCP Valley of Pyrrhotite, Smythite, and Marcasite. Smythite ($Fe_{3+x}S_4$) and marcasite (o-FeS_2) are challenging materials to synthesize. Fast-reacting thioureas can nucleate into the hexagonal valley but always with concomitant nucleation of ccp phases. Alternatively, the mountain pass is a second route to access the hcp valley. Using the landscape described, it appears that two different sets of reaction conditions are needed in succession: first, one with low sulfur reactivity and high temperature, followed by one with high sulfur reactivity. There is only one other reported colloidal synthesis of marcasite (o-FeS_2), which coincidentally also had two sulfur sources of differing reactivity.[38]

First, to achieve pyrrhotite ($Fe_{1-x}S$), a low reactivity sulfur reagent, such as diphenylthiourea, is needed to avoid the mackinawite ($Fe_{1+x}S$) to greigite (Fe_3S_4) and pyrite (FeS_2) transformation path. High temperatures (245 °C) are needed to convert ccp mackinawite ($Fe_{1+x}S$) nuclei over the mountain pass to the slightly more stable hcp pyrrhotite ($Fe_{1-x}S$). These conditions gave pyrrhotite in a pure form within the limitations of powder diffraction. We did not observe the stoichiometric endmember of the pyrrhotite family, troilite (FeS), under these conditions likely due to the excess of sulfur reagent employed.

In a second step and in parallel approach to achieving pyrite, more reactive sulfur is needed to convert the pyrrhotite ($Fe_{1-x}S$) exclusively to smythite ($Fe_{3+x}S_4$) and marcasite (o-FeS_2). Using a second addition of 3:1 acetylthiourea/Fe at 160 °C gave 30% pyrrhotite and 70% smythite ($Fe_{3+x}S_4$). Increasing the reaction temperature of this second step to 245 °C gave predominantly marcasite (o-FeS_2).

https://doi.org/10.1021/jacs.3c05653
J. Am. Chem. Soc. 2023, 145, 18948−18955

It was found that the proportion of marcasite could be increased by adding and substituting the ODE solvent with oleylamine in the first step. Oleylamine substitutes the thiourea in situ (Supporting Information) to give a very slow-reacting thiourea. These conditions seemed to give a highly crystalline pyrrhotite intermediate, which in turn yielded 82% marcasite with only 18% pyrite impurity.

CONCLUSIONS

By using a library of thioureas with tunable reactivity, we were able to observe all eight of the known iron sulfides as products and a semicrystalline phase. Fast-reacting thioureas, such as unsubstituted thiourea, gave a complex mixture of iron sulfides. At low temperatures of 170 °C, sulfur-poor phases dominate, especially ∼FeS phases. At high temperatures of 245 °C, sulfur-rich phases dominate including pyrite and marcasite (FeS_2). With medium-reacting thioureas, such as acetylthiourea, at low temperature, greigite (Fe_3S_4) dominates and is replaced by pyrite (FeS_2) at high temperatures. With slow-reacting thioureas, such as diphenylthiourea, at low temperatures, mackinawite ($Fe_{1+x}S$) and greigite (Fe_3S_4) form, yet at high temperatures, pyrrhotite ($Fe_{1-x}S$) dominates.

Using these experiments, we developed the first ever synthetic phase diagram to visualize the trends among thiourea reactivity, reaction temperature, and sulfur content in the product phases observed. We hypothesize that the anion stacking of the nucleated sulfur-poor phase is a large determinant in the paths subsequently taken to the other phases of differing stoichiometry. Most notably, this study is the first of its kind to strategically and rationally target specific phases in iron sulfides. Here, we show that it is imperative to consider both synthetic mechanisms, decomposition pathways, crystal structures, and phase transformation pathways when targeting the desired structure. This understanding of phase control can be applied to other compound materials, enabling their targeted synthesis and will ultimately contribute to further development of a wide range of technologies requiring crystalline materials.

ASSOCIATED CONTENT

Supporting Information

The Supporting Information is available free of charge at https://pubs.acs.org/doi/10.1021/jacs.3c05653.

Rietveld refinements, NMR spectra, additional methods, and supporting experiments (PDF)

AUTHOR INFORMATION

Corresponding Author

Janet E. Macdonald − *Department of Chemistry, Vanderbilt University, Nashville, Tennessee 37235, United States; Vanderbilt Institute of Nanoscale Science and Engineering, Vanderbilt University, Nashville, Tennessee 37235, United States;* orcid.org/0000-0001-6256-0706; Email: Janet.Macdonald@vanderbilt.edu

Author

Jeremy R. Bairan Espano − *Department of Chemistry, Vanderbilt University, Nashville, Tennessee 37235, United States; Vanderbilt Institute of Nanoscale Science and Engineering, Vanderbilt University, Nashville, Tennessee 37235, United States;* orcid.org/0000-0001-7571-337X

Complete contact information is available at: https://pubs.acs.org/10.1021/jacs.3c05653

Funding

The authors thank the US National Science Foundation for support through CHE1905265 and CHE2305161.

Notes

The authors declare no competing financial interest.

ABBREVIATIONS

XRD, CC X-ray diffraction; o, CC orthorhombic

REFERENCES

(1) Jain, A.; Ong, S. P.; Hautier, G.; Chen, W.; Richards, W. D.; Dacek, S.; Cholia, S.; Gunter, D.; Skinner, D.; Ceder, G.; Persson, K. A. Commentary: The materials project: A materials genome approach to accelerating materials innovation. *APL Mater.* **2013**, *1* (1), No. 011002.

(2) Lennie, A. R.; Vaughan, D. J. Spectroscopic studies of iron sulfide formation and phase relations at low temperatures. *Miner. Spectrosc.: Tribute Roger G. Burns* **1996**, No. 5, 117−131.

(3) Hendricks, M. P.; Campos, M. P.; Cleveland, G. T.; Plante, I. J.-L.; Owen, J. S. A Tunable library of substituted thiourea precursors to metal sulfide nanocrystals. *Science* **2015**, *348* (6240), 1226−1230.

(4) Hollingsworth, N.; Roffey, A.; Islam, H. U.; Mercy, M.; Roldan, A.; Bras, W.; Wolthers, M.; Catlow, C. R. A.; Sankar, G.; Hogarth, G.; de Leeuw, N. H. Active nature of primary amines during thermal decomposition of nickel dithiocarbamates to nickel sulfide nanoparticles. *Chem. Mater.* **2014**, *26* (21), 6281−6292.

(5) Thomson, J. W.; Nagashima, K.; MacDonald, P. M.; Ozin, G. A. From sulfur-amine solutions to metal sulfide nanocrystals: Peering into the oleylamine-sulfur black box. *J. Am. Chem. Soc.* **2011**, *133* (13), 5036−5041.

(6) Frenette, L. C.; Krauss, T. D. Uncovering active precursors in colloidal quantum dot synthesis. *Nat. Commun.* **2017**, *8* (1), No. 2082.

(7) Rhodes, J. M.; Jones, C. A.; Thal, L. B.; Macdonald, J. E. Phase-controlled colloidal syntheses of iron sulfide nanocrystals via sulfur precursor reactivity and direct pyrite precipitation. *Chem. Mater.* **2017**, *29* (19), 8521−8530.

(8) Bi, Y.; Yuan, Y.; Exstrom, C. L.; Darveau, S. A.; Huang, J. Air stable, photosensitive, phase pure iron pyrite nanocrystal thin films for photovoltaic application. *Nano Lett.* **2011**, *11* (11), 4953−4957.

(9) Fan, H. H.; Li, H. H.; Huang, K. C.; Fan, C. Y.; Zhang, X. Y.; Wu, X. L.; Zhang, J. P. Metastable Marcasite-FeS2 as a New Anode Material for Lithium Ion Batteries: CNFs-Improved Lithiation/Delithiation Reversibility and Li-Storage Properties. *ACS Appl. Mater. Interfaces* **2017**, *9* (12), 10708−10716.

(10) Chang, Y. S.; Savitha, S.; Sadhasivam, S.; Hsu, C. K.; Lin, F. H. Fabrication, characterization, and application of greigite nanoparticles for cancer hyperthermia. *J. Colloid Interface Sci.* **2011**, *363* (1), 314−319.

(11) Rickard, D.; Luther, G. W. Chemistry of iron sulfides. *Chem. Rev.* **2007**, *107* (2), 514−562.

(12) Waldner, P.; Pelton, A. D. Thermodynamic modeling of the Fe-S system. *J. Phase Equilib. Diffus.* **2005**, *26* (1), 23−38.

(13) Grønvold, F.; Westrum, E. F. Heat capacities of iron disulfides Thermodynamics of marcasite from 5 to 700 K, pyrite from 300 to 780 K, and the transformation of marcasite to pyrite. *J. Chem. Thermodyn.* **1976**, *8* (11), 1039−1048.

(14) Anderko, A.; Shuler, P. J. A computational approach to predicting the formation of iron sulfide species using stability diagrams. *Comput. Geosci.* **1997**, *23* (6), 647−658.

(15) Chase, M. W.; Curnutt, J. L.; Downey, J. R.; McDonald, R. A.; Syverud, A. N.; Valenzuela, E. A. JANAF Thermochemical Tables, 1982 Supplement. *J. Phys. Chem. Ref. Data* **1982**, *11* (3), 695−940.

(16) Vaughan, D. J.; Lennie, A. R. The iron sulphide minerals: their chemistry and role in nature. *Science Progress* **1991**, *75* (3−4), 371−388.
(17) Berner, R. A. Thermodynamic Stability of Sedimentary Iron Sulfides. *Am. J. Sci.* **1967**, *265* (9), 773−785.
(18) de Médicis, R. Cubic FeS, a Metastable Iron Sulfide. *Science* **1970**, *170* (3963), 1191−1192.
(19) Subramani, T.; Lilova, K.; Abramchuk, M.; Leinenweber, K. D.; Navrotsky, A. Greigite (Fe3S4) is thermodynamically stable: Implications for its terrestrial and planetary occurrence. *Proc. Natl. Acad. Sci. U.S.A.* **2020**, *117* (46), 28645−28648.
(20) Hoffmann, V. Greigite (Fe3S4): magnetic properties and first domain observations. *Phys. Earth Planet. Inter.* **1992**, *70*, 288−301.
(21) Erd, R.; Evans, H.; Richter, D. Smythite, a New Iron Sulfide, and Associated Pyrrhotite From Indiana. *Am. Mineral.* **1957**, *42*, 309−333.
(22) Kaur, G.; Kaur, M.; Thakur, A.; Kumar, A. Recent Progress on Pyrite FeS2 Nanomaterials for Energy and Environment Applications: Synthesis, Properties and Future Prospects. *J. Cluster Sci.* **2020**, *31*, 899−937, DOI: 10.1007/s10876-019-01708-3.
(23) Murowchick, J. B.; Barnes, H. L. Formation of cubic FeS. *Am. Mineral.* **1986**, *71* (9−10), 1243−1246.
(24) Bourdoiseau, J. A.; Jeannin, M.; Rémazeilles, C.; Sabot, R.; Refait, P. The transformation of mackinawite into greigite studied by Raman spectroscopy. *J. Raman Spectrosc.* **2011**, *42* (3), 496−504.
(25) Hunger, S.; Benning, L. G. Greigite: A true intermediate on the polysulfide pathway to pyrite. *Geochem. Trans.* **2007**, *8*, 1−20.
(26) Novikov, G. V.; Egorov, V. K.; Popov, V. I.; Sipavina, L. V. Kinetics and mechanism of transformations in iron-rich pyrrhotites and in troilite-pyrrhotite metastable assemblages. *Phys. Chem. Miner.* **1977**, *1* (1), 1−14.
(27) Furukawa, Y.; Barnes, H. L. Reactions forming smythite, Fe9S11. *Geochim. Cosmochim. Acta* **1996**, *60* (19), 3581−3591.
(28) Bai, P.; Zheng, S.; Chen, C.; Zhao, H. Investigation of the iron-sulfide phase transformation in nanoscale. *Cryst. Growth Des.* **2014**, *14* (9), 4295−4302.
(29) Ostwald, W. Studien über die Bildung und Umwandlung fester Körper 1. Abhandlung: Übersättigung und Überkaltung. *Z. Phys. Chem.* **1897**, *22*, 289−330.
(30) Sun, W.; Dacek, S. T.; Ong, S. P.; Hautier, G.; Jain, A.; Richards, W. D.; Gamst, A. C.; Persson, K. A.; Ceder, G. The thermodynamic scale of inorganic crystalline metastability. *Sci. Adv.* **2016**, *2* (11), No. e1600225.
(31) Lennie, A. R.; England, K. E. R.; Vaughan, D. J. Transformation of synthetic mackinawite to hexagonal pyrrhotite: a kinetic study. *Am. Mineral.* **1995**, *80* (9−10), 960−967.
(32) Wilkin, R. T.; Barnes, H. L. Pyrite formation by reactions of iron monosulfides with dissolved inorganic and organic sulfur species. *Geochim. Cosmochim. Acta* **1996**, *60* (21), 4167−4179.
(33) Kitchaev, D. A.; Ceder, G. Evaluating structure selection in the hydrothermal growth of FeS 2 pyrite and marcasite. *Nat. Commun.* **2016**, *7*, No. 13799.
(34) Csákberényi-Malasics, D.; Rodriguez-Blanco, J. D.; Kis, V. K.; Rečnik, A.; Benning, L. G.; Pósfai, M. Structural properties and transformations of precipitated FeS. *Chem. Geol.* **2012**, *294−295*, 249−258.
(35) Matamoros-Veloza, A.; Cespedes, O.; Johnson, B. R. G.; Stawski, T. M.; Terranova, U.; de Leeuw, N. H.; Benning, L. G. A highly reactive precursor in the iron sulfide system. *Nat. Commun.* **2018**, *9* (1), No. 3125.
(36) Beauvais, M. L.; Chupas, P. J.; O'Nolan, D.; Parise, J. B.; Chapman, K. W. Resolving Single-layer Nanosheets as Short-lived Intermediates in the Solution Synthesis of FeS. *ACS Mater. Lett.* **2021**, *3* (6), 698−703.
(37) Moreau, L. M.; Ha, D.-H.; Zhang, H.; Hovden, R.; Muller, D. A.; Robinson, R. D. Defining Crystalline/Amorphous Phases of Nanoparticles through X-ray Absorption Spectroscopy and X-ray Diffraction: The Case of Nickel Phosphide. *Chem. Mater.* **2013**, *25* (12), 2394−2403.
(38) Li, T.; Guo, Z.; Li, X.; Wu, Z.; Zhang, K.; Liu, H.; Sun, H.; Liu, Y.; Zhang, H. Colloidal synthesis of marcasite FeS2 nanoparticles with improved electrochemical performance. *RSC Adv.* **2015**, *5* (120), 98967−98970.

https://doi.org/10.1021/jacs.3c05653
J. Am. Chem. Soc. 2023, 145, 18948−18955